Supplemental Material for

Extending the Human Connectome Project across ages: Imaging protocols for the Lifespan Development and Aging projects

Michael P. Harms*[a], Leah H. Somerville*[f,g], Beau M. Ances[b], Jesper Andersson[h], Deanna M. Barch[a,c,e], Matteo Bastiani[h], Susan Y. Bookheimer[k], Timothy B. Brown[c], Randy L. Buckner[f,g,m,n], Gregory C. Burgess[a], Timothy S. Coalson[d], Michael A. Chappell[h,i], Mirella Dapretto[k], Gwenaëlle Douaud[h], Bruce Fischl[m,o], Matthew F. Glasser[c,d,p], Douglas N. Greve[m], Cynthia Hodge[a], Keith W. Jamison[q], Saad Jbabdi[h], Sridhar Kandala[a], Xiufeng Li[r], Ross W. Mair[g,m], Silvia Mangia[r], Daniel Marcus[c], Daniele Mascali[t], Steen Moeller[r], Thomas E. Nichols[h,j,u], Emma C. Robinson[v], David H. Salat[m], Stephen M. Smith[h], Stamatios N. Sotiropoulos[h,w], Melissa Terpstra[r], Kathleen M. Thomas[s], M. Dylan Tisdall[x], Kamil Ugurbil[r], Andre van der Kouwe[m,n], Roger P. Woods[k,l], Lilla Zöllei[m], David C. Van Essen[d], & Essa Yacoub[r]

* Equal first author contribution

Departments of Psychiatry[a], Neurology[b], Radiology[c], and Neuroscience[d], Washington University School of Medicine, St. Louis, MO USA
Department of Psychological and Brain Sciences[e], Washington University in St. Louis, St. Louis, MO USA
Department of Psychology[f] and Center for Brain Science[g], Harvard University, Cambridge, MA USA
Wellcome Centre for Integrative Neuroimaging, Oxford Centre for Functional Magnetic Resonance Imaging of the Brain (FMRIB), Nuffield Department of Clinical Neurosciences[h], University of Oxford, Oxford, UK
Institute of Biomedical Engineering, Department of Engineering Science[i], University of Oxford, Oxford, UK
Oxford Big Data Institute, Li Ka Shing Centre for Health Information and Discovery, Nuffield Department of Population Health[j], University of Oxford, Oxford, UK
Departments of Psychiatry and Biobehavioral Sciences[k] and Neurology[l], David Geffen School of Medicine at UCLA, University of California, Los Angeles, CA USA
Athinoula A. Martinos Center for Biomedical Imaging, Department of Radiology[m] and Department of Psychiatry[n], Massachusetts General Hospital, Harvard Medical School, Boston, MA USA
Computer Science and Artificial Intelligence Laboratory[o], Massachusetts Institute of Technology, Cambridge, MA USA
St. Luke's Hospital[p], St. Louis, MO USA
Department of Radiology[q], Weill Cornell Medical College, New York, NY USA
Center for Magnetic Resonance Imaging[r] and Institute of Child Development[s], University of Minnesota, Minneapolis, MN USA
Centro Fermi - Museo Storico della Fisica e Centro Studi e Ricerche "Enrico Fermi"[t], Rome, Italy
Department of Statistics[u], University of Warwick, Coventry, UK
Department of Biomedical Engineering[v], King's College London, London, UK
Sir Peter Mansfield Imaging Centre[w], School of Medicine, University of Nottingham, Nottingham, UK
Department of Radiology[x], Perelman School of Medicine, University of Pennsylvania, Philadelphia, PA US

Supplemental Text

MRI Hardware

During pilot testing we compared the Siemens 32-channel (ch) head coil with the 64-ch head/neck coil. We found no compelling reasons to switch from the 32-ch coil (used for HCP-YA) to the 64-ch coil in terms of SNR across the whole brain. This was not surprising given that the 64-ch coil has a slightly larger form factor and only a few more coil elements specific to the 'head' portion of the coil (40 head elements; 24 neck elements). Thus, we continued using the 32-ch head coil as the primary HCP-D/A coil.

We are currently investigating a pediatric 32-ch head coil developed by Ceresensa [http://www.ceresensa.com] for scanning of 5-7 year old participants. This coil has a smaller inner diameter than the Siemens 32-ch coil and a hinged top (anterior) compartment, yielding an open design above the participant's eyes and face. Given budget constraints and for efficiency, we would use two Ceresensa coils (at the Washington University and UCLA sites) to acquire all the data from 5-7 year olds. See Supplemental Figure 1 for pilot data from a preliminary version of this coil. Further testing of a modified version of this coil is pending. While there are drawbacks to using two different head coils across the study sample, this approach may be preferable for dealing with the challenges posed by the smaller head and neck length of young children (i.e., getting their heads centered comfortably in the 'sweet spot' of the coil, and ensuring unobstructed viewing of the mounted mirror and visual stimuli).

Supplemental Figures

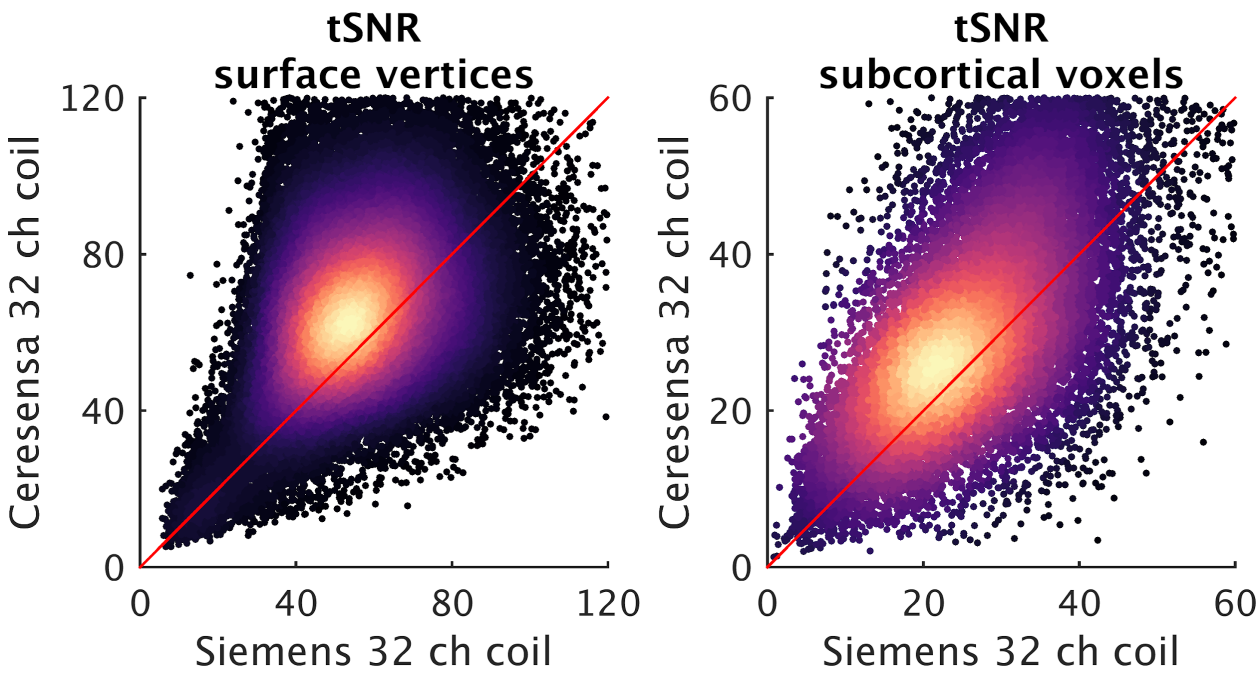

Supplemental Figure 1. Scatterplots of temporal SNR (tSNR) of surface vertices (left panel) and subcortical voxels (right panel) in a preliminary version of the Ceresensa 32-channel (ch) pediatric head coil versus the Siemens 32-ch adult head coil, colored according to the relative density of the points (black = low density; light yellow = highest density). A single adult subject with a small head completed a resting state fMRI scan (488 frames, 6.5 min, 'AP' phase encoding polarity) in both head coils. The scans were processed with the HCP 'minimal-preprocessing' pipeline to yield a 2 mm standard grayordinate (CIFTI) representation (59412 surface vertices and 31870 'subcortical' voxels, including cerebellum), from which tSNR for each grayordinate was computed (mean signal over time divided by the standard deviation over time). The subject (female, 38 years old) had minimal movement during both scans. Note the differing ranges of the axes between the two panels. The red diagonal line is the line of identity.

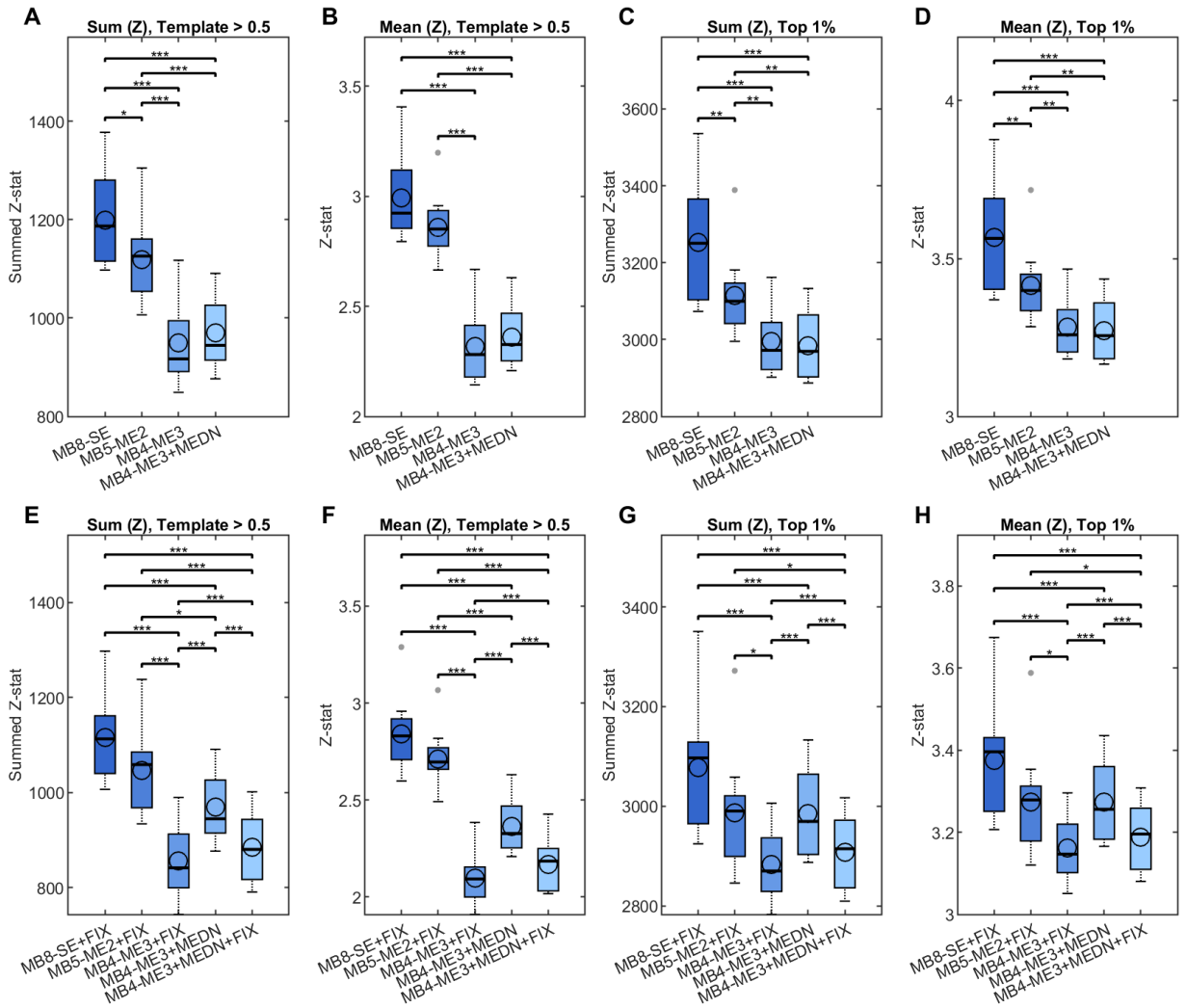

Supplemental Figure 2. Additional measures from the evaluation of multiband multi-echo (MB-ME) pilot data. The acquisition/processing variants and figure layout are the same as Figure 2 in the main text (with non-FIX'ed data in top row, and FIX'ed data in bottom row) except the measures are now the sum and mean mixture-model-corrected (MMC) Z-stat derived from either a common spatial mask (defined for each resting-state network (RSN) as the grayordinates with value > 0.5 in the RSN templates used for the dual-regression) (panels A,B,E,F) or from the top 1% of MMC Z-stat values (C,D,G,H). The average number of grayordinates in the common spatial mask (across the 100 RSN templates) was 423 (std=294; out of 91282 grayordinates). The choice of 1% as the 'threshold' for the other alternative quantification was based on the fact that 913 grayordinates (1% of 91282) is similar to the approximately 600-1200 grayordinates selected when we used the MMC equal probability threshold between activation and noise (see Fig. 2A and 2F in main text). Note that the sum and mean when using the top 1% to select the grayordinates are scaled replicas of each other (C vs. D, and G vs. H), but both are provided for completeness. (The sum and mean are not strictly scaled replicas when using Template > 0.5 to select the grayordinates because that criterion selects differing numbers of grayordinates across the 100 RSN templates). By using a common spatial mask and the top 1% of grayordinates the ensuing results are independent of the differences between acquisition/processing variants in the MMC equal probability threshold (Fig. 2E and 2J). The results of these measures are broadly consistent with the results in Figure 2 in that the highest values are obtained for the MB8-SE data.

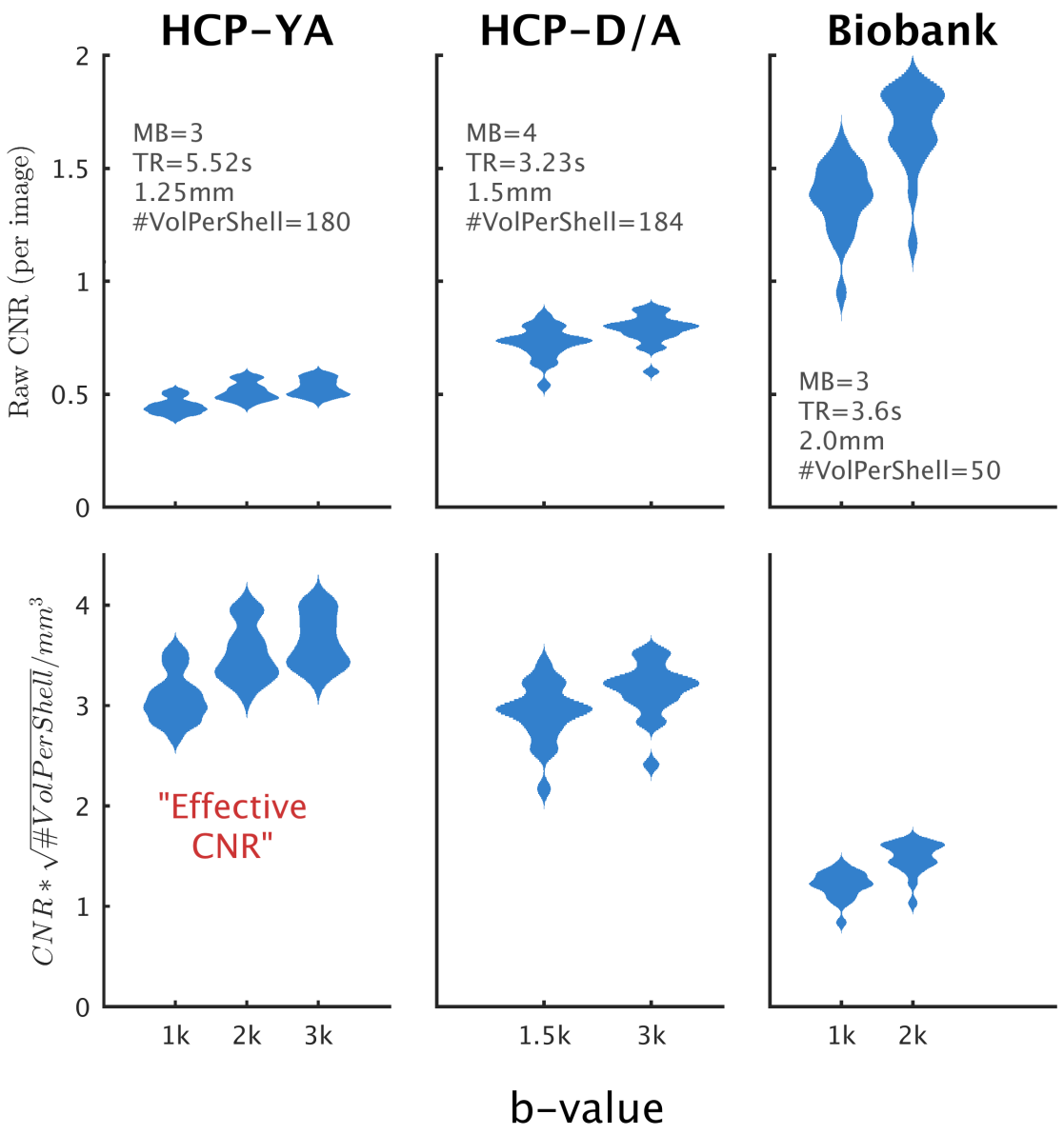

Supplemental Figure 3. Violin plots (smoothed histograms) of the contrast-to-noise (CNR) by b-value from 18-19 subjects of the dMRI data collected with the HCP-YA, HCP-D/A, and UK Biobank protocols (mean age of 28, 18, and 61 years, respectively). Raw CNR and effective CNR were computed as defined in Figure 3 (main text) except the ROI for the computation was over the whole white matter. The Biobank protocol has the largest raw CNR of the compared protocols due to its larger voxel volume (137% larger than HCP-D/A). The HCP-D/A dMRI protocol has a favorable, albeit slightly lower, effective CNR compared to the HCP-YA protocol, consistent with the fact that the HCP-D/A protocol collects approximately the same number of volumes *per shell* (although HCP-YA collected 3 shells, rather than 2 for HCP-D/A), but has a 73% larger voxel volume compared to HCP-YA (and thus is "penalized" relative to HCP-YA by the normalization by voxel volume). HCP-YA data were collected on the Siemens 3T customized 'Connectom' scanner (100 mT/m gradients); HCP-D/A data on a Siemens 3T Prisma (80 mT/m gradients); Biobank on a Siemens 3T Skyra (45 mT/m gradients). All protocols used a partial Fourier factor of 6/8, and no in-plane (phase) acceleration.

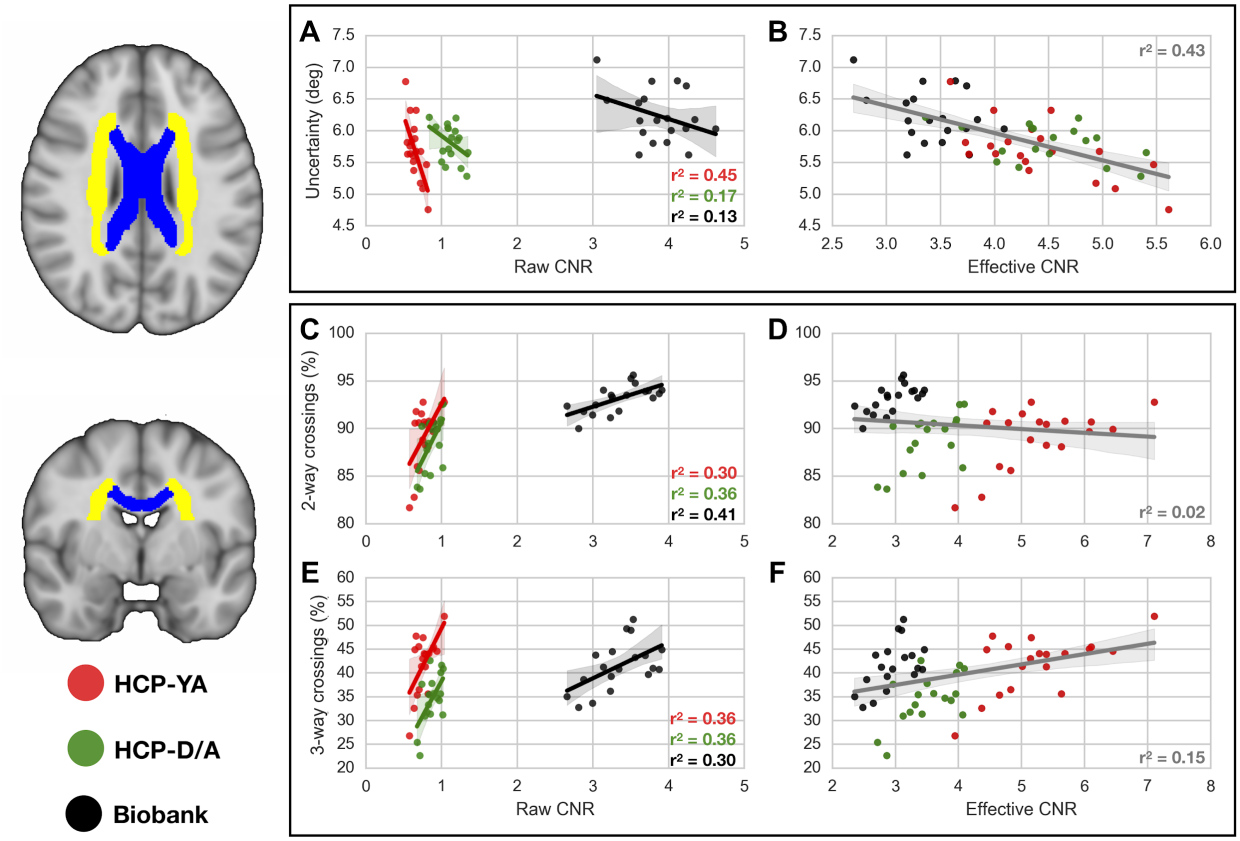

Supplemental Figure 4. Comparison between 3 different dMRI protocols in terms of CNR, fiber orientation uncertainty, and detection of 2- and 3-way fiber crossings. See Figure 3 (main text) for details of the measures and analysis. Relative to Figure 3, data from 19 participants in the UK Biobank project (mean age 61 years) have been added. The Biobank dMRI protocol uses larger (2.0 mm isotropic) voxels, which explains its considerably higher values of raw CNR in both the corpus callosum (A) and centrum semiovale (C,E). However, because of its considerably shorter scan duration, the effective CNR of the Biobank dMRI protocol is lower than that of the HCP-YA and HCP-D/A dMRI protocols (B,D,F; see also Supplemental Figure 3). The regression line between effective CNR and uncertainty computed using the data from all 3 protocols (B) is very similar to that obtained using the data from just the HCP-YA and HCP-D/A protocols (i.e., compare to regression line in Fig. 3B), and visually the regression line for effective CNR and uncertainty appears to fit the data from each protocol equally well (e.g., roughly equal number of points above and below the regression line for each protocol). However, this is not the case for the inclusion of the Biobank data into the regression between effective CNR and the percentage of 2-way (D) and 3-way (F) crossings (i.e., compare to the regression lines in Fig. 3D and 3F), indicating that effects related to age differences may be impacting the relationship or simply that as protocol differences increase, the simplistic adjustments involved in “effective CNR” are not sufficient.

Supplemental Table 1. 'Minimal preprocessing' procedures for publicly released data

PIPELINE	GOALS/OUTPUTS
STRUCTURAL PRIMARY INPUTS: 1) NIFTI format T1w volume; 2) NIFTI format T2w volume	
PreFreeSurfer	1) Produce an undistorted "native" structural volume space for each subject. This includes removing gradient-nonlinearity-induced distortions and readout direction distortions. 2) Align the T1w and T2w 3) Perform a correction of the receive-coil bias field 4) Register the subject's native structural volume space to MNI space using FSL's FNIRT
FreeSurfer	1) Segment the volume into predefined structures 2) Derive the white and pial cortical surfaces
PostFreeSurfer	1) Produce all the volume and surface files necessary for viewing data in Connectome Workbench 2) Perform 'MSMSulc' surface registration[a] to the Conte69 surface template 3) Downsample registered surfaces for connectivity analysis 4) Create final brain mask 5) Create myelin maps
FUNCTIONAL PRIMARY INPUTS: 1) Resting state and task-based functional scans (fMRI), 2) Output from Structural Preprocessing	
fMRIVolume	1) Remove spatial distortions 2) Realign volumes to correct for subject motion 3) Register fMRI data to structural data 4) Reduce the receive-coil bias field 5) Normalize data to global mean 6) Mask data with the final brain mask
fMRISurface	1) Bring the volumetric time series into the CIFTI grayordinates standard space with a small amount (2 mm full-width-half-max) of appropriate spatial smoothing (surface smoothing for the vertices; parcel constrained smoothing for subcortical voxels) 2) Result is a standard set of grayordinates in every subject with 2 mm average surface vertex and subcortical volume voxel spacing
DIFFUSION PRIMARY INPUTS: 1) Diffusion scans (dMRI), 2) Output from Structural Preprocessing	
Diffusion	1) Normalize the image intensity across runs so that there is a consistent average b_0 intensity in each run 2) Remove EPI distortions 3) Remove eddy-current-induced distortions 4) Reduce subject motion distortions 5) Remove gradient-nonlinearity distortions 6) Register to structural data 7) Mask data with the final brain mask

[a] 'MSMSulc' registration uses FreeSurfer's "sulc" map with the Multimodal Surface Matching (MSM) algorithm to derive a surface alignment based on cortical folding, but with less distortion than the native spherical registration within FreeSurfer {Robinson, 2014 #3318;Robinson, 2018 #3384}.

References

Robinson, E.C., Garcia, K., Glasser, M.F., Chen, Z., Coalson, T.S., Makropoulos, A., Bozek, J., Wright, R., Schuh, A., Webster, M., Hutter, J., Price, A., Cordero Grande, L., Hughes, E., Tusor, N., Bayly, P.V., Van Essen, D.C., Smith, S.M., Edwards, A.D., Hajnal, J., Jenkinson, M., Glocker, B., Rueckert, D., 2018. Multimodal surface matching with higher-order smoothness constraints. Neuroimage 167, 453-465.

Robinson, E.C., Jbabdi, S., Glasser, M.F., Andersson, J., Burgess, G.C., Harms, M.P., Smith, S.M., Van Essen, D.C., Jenkinson, M., 2014. MSM: a new flexible framework for Multimodal Surface Matching. Neuroimage 100, 414-426.